

# Quasiparticle self-consistent $GW$ study of cuprates: electronic structure, model parameters, and the two-band theory for $T_c$

Seung Woo Jang,<sup>1</sup> Takao Kotani,<sup>2</sup> Hiori Kino,<sup>3</sup> Kazuhiko Kuroki,<sup>4</sup> and Myung Joon Han<sup>1,5,\*</sup>

<sup>1</sup>*Department of Physics, Korea Advanced Institute of Science and Technology (KAIST), Daejeon 305-701, Korea*

<sup>2</sup>*Department of Applied Mathematics and Physics, Tottori University, Tottori 680-8552, Japan*

<sup>3</sup>*National Institute for Materials Science, Sengen 1-2-1, Tsukuba, Ibaraki 305-0047, Japan.*

<sup>4</sup>*Department of Physics, Osaka University, Machikaneyama-Cho, Toyonaka, Osaka 560-0043, Japan*

<sup>5</sup>*KAIST Institute for the NanoCentury, Korea Advanced Institute of Science and Technology, Daejeon 305-701, Korea*

## Abstract

Despite decades of progress, an understanding of unconventional superconductivity still remains elusive. An important open question is about the material dependence of the superconducting properties. Using the quasiparticle self-consistent  $GW$  method, we re-examine the electronic structure of copper oxide high- $T_c$  materials. We show that QSGW captures several important features, distinctive from the conventional LDA results. The energy level splitting between  $d_{x^2-y^2}$  and  $d_{3z^2-r^2}$  is significantly enlarged and the van Hove singularity point is lowered. The calculated results compare better than LDA with recent experimental results from resonant inelastic x-ray scattering and angle resolved photoemission experiments. This agreement with the experiments supports the previously suggested two-band theory for the material dependence of the superconducting transition temperature,  $T_c$ .

---

\*Electronic address: mj.han@kaist.ac.kr

After the seminal work of finding high temperature superconductivity in a ceramic copper oxide material [1], efforts to understand the cuprate have long been a central part of modern condensed matter physics. Although many intriguing aspects of its electronic behaviors have been unveiled and great progress has been made, an understanding of its superconducting mechanism, the novel interplay between competing phases, and its relationship to other correlated phenomena is still far from clear [2–12]. One simple, well-defined but still open question is what determines the superconducting transition temperature ( $T_c$ ), or its material dependency. For example, the  $T_c$  of the single layer cuprates can be different by a factor of two;  $\sim 40\text{K}$  for  $\text{La}_2\text{CuO}_4$  and  $\sim 90\text{K}$  for  $\text{HgBa}_2\text{CuO}_4$ . On the one hand, it may be too early to ask this question, while the superconducting mechanism itself still remains elusive. On the other, however, figuring out the detailed features behind the material dependency can provide the crucial hint for further understanding of superconductivity and other related properties. In fact, many directly or indirectly related theoretical studies have been performed on this issue [13–25].

In this regard, a notable suggestion has recently been made [26–29]. According to this theory, the  $T_c$  of the single-layer cuprate can be described with a two-orbital model that considers both the  $d_{x^2-y^2}$  and  $d_{3z^2-r^2}$  Wannier orbitals, and the energy level offset between the two orbitals,  $\Delta E$ , plays a key role in determining  $T_c$ . Whereas the larger value of this energy separation produces the higher  $T_c$  (*e.g.*, the case of  $\text{HgBa}_2\text{CuO}_4$ ) due to the better one band feature achieved, the smaller value results in the lower  $T_c$  (*e.g.*, the case of  $\text{La}_2\text{CuO}_4$ ) in spite of the better nested Fermi surface. The calculated Eliashberg parameter ( $\lambda$ ) based on the many-body calculation using the fluctuating exchange (FLEX) approximation [30, 31] clearly exhibits a linear dependence on  $\Delta E$  while the other parameters are shown to be less important. Further, this theory can be extended to the bilayer case [29], which explains the correlation between the Fermi surface shape and  $T_c$  [24].

A possible experimental test to verify this two-band theory is to examine the correlation between  $T_c$  and  $\Delta E$ , the Fermi surface shape, or the partial density of states of the  $d_{3z^2-r^2}$  orbital, which can be measured by recent techniques such as resonant inelastic xray scattering (RIXS), and (angle resolved) photoemission spectroscopy (ARPES). However, while the theoretical  $\Delta E$  or the Fermi surface shape was obtained from the LDA and used as the “inputs” for the many-body FLEX calculation in Refs. 26–29, the experimentally determined  $\Delta E$  and the Fermi surface shape should be regarded as the “outputs” or “results” after the

consideration of the many-body correlation effects beyond LDA/GGA. In fact, while a RIXS study reports that  $T_c$  is higher for larger  $\Delta E$  [32], the actual experimental value of  $\Delta E$  is larger than the theoretical evaluation, presumably due to this “input vs. output” problem. One possible way to resolve this problem, at least partially, is to re-evaluate  $\Delta E$  as an output of the FLEX calculation. However, this approach would suffer from various ambiguities regarding the Hubbard interaction strength and the definition of the renormalized  $\Delta E$ . It is problematic since a quantitative comparison is required in between the theory and experiment, while only the qualitative comparison was made regarding  $T_c$  in Refs. 26–29.

In the present paper, we use a first-principles approach, exploiting the quasiparticle self-consistent  $GW$  (QSGW) method. It enables us to take into account the correlation effects beyond LDA/GGA. In this way, we can obtain a well-defined renormalized  $\Delta E$  without introducing adjustable parameters.

In Ref. 17, a quantum chemical approach was adopted to evaluate the energy level offset between Cu- $d_{x^2-y^2}$  and  $d_{3z^2-r^2}$  orbitals, where the correlation effects were taken into account within a cluster-based configuration-interaction-type calculation. A good agreement with the RIXS experiment was found by assuming the energy difference of ferromagnetically and antiferromagnetically ordered states to be  $2J$ , where  $J$  is the antiferromagnetic coupling constant. Our approach is fairly different and is along the line of the first-principles band calculation as in Refs. 26–29. In the sense mentioned above, the calculated  $\Delta E$  can be compared to the experiments, while it should not be regarded as an input parameter for the many-body calculation, because doing so would result in a partial double counting of the correlation effects. Still, the present approach can also provide a first-step hint toward obtaining a better “non-interacting” Hamiltonian that can be used as an input for the many-body calculation of superconductivity. In fact, it is known that the non-interacting Hamiltonian obtained from LDA has a problem when used as an input for the FLEX calculation, and the LDA/GGA estimation of  $\Delta E$  for  $\text{La}_2\text{CuO}_4$  is too small to account for the maximum  $T_c$  of 40K in the  $\text{La}_2\text{CuO}_4$  [33]. In this context, it is worth pointing out that the  $GW$  method has been successfully applied to the many of strongly correlated materials in combination with, for example, dynamical mean field theory (DMFT) [34–37].

## Results and Discussion

To our knowledge, there is no previous QSGW study for the cuprate band structure although it has been discussed conceptually [38]. Here we first examine the electronic structure and the two-band theory for the material-dependent  $T_c$  of a single layer cuprate. While the QSGW calculation produces notable differences in the band structure and Fermi surface from LDA, the two-band explanation for  $T_c$  still remains valid. QSGW results of model parameters are presented and compared to the RIXS data as well as the LDA calculations. It clearly shows that the parameters produced by QSGW are in better agreement with the experiment. Finally, we investigate the epitaxially strained  $\text{La}_2\text{CuO}_4$  whose noticeable  $T_c$  increase has been previously reported. Two-band theory also works well for this situation.

### Electronic structure and the $T_c$ of single layer compounds

Fig. 1(a) and (b) show the band dispersion and projected density of states (PDOS) of  $\text{La}_2\text{CuO}_4$  calculated by LDA and QSGW, respectively. The LDA result is in good agreement with the previous calculation (see, for example, Ref. 26 and Ref. 27). In the QSGW, several important differences are noted. First, the band width of both  $e_g$  orbitals are significantly reduced, by about 1.30 and 0.65 eV for  $d_{x^2-y^2}$  and  $d_{3z^2-r^2}$ , respectively, indicating that the band width overestimation (or effective mass underestimation) problem of LDA is somehow overcome by the QSGW procedure. Another key difference is that the separation between the  $d_{x^2-y^2}$  and  $d_{3z^2-r^2}$  bands becomes larger in QSGW, as seen in Fig. 1(b). The  $d_{x^2-y^2}$  energy level,  $E_{x^2-y^2}$ , is shifted from  $-0.14$  (LDA) to  $-0.03$  (QSGW) while  $E_{3z^2-r^2}$  is from  $-0.98$  (LDA) to  $-1.68$  (QSGW) (indicated by the arrows in Fig. 1; see also Table I). It is a factor of two difference in  $\Delta E_{e_g}$ ; 0.84 eV in LDA and 1.66 in QSGW. The correct estimation of this quantity is important especially in the two-band theory for  $T_c$  [26–29]. The large value of  $\Delta E_{e_g}$  is indeed consistent with the RIXS data as will be discussed further below.

The same features are also found in  $\text{HgBa}_2\text{CuO}_4$ , as presented in Fig. 1(c) and (d). The  $d_{x^2-y^2}$  band width is reduced by  $\sim 0.75$  eV in QSGW compared to LDA and its center position of PDOS moves slightly upward by 0.15 eV. While the  $d_{3z^2-r^2}$  dispersion in this material is already quite small due to the thicker blocking layer, its band width in QSGW is further reduced.  $\Delta E_{e_g}$  is 2.25 in QSGW, again noticeably larger than the LDA value of

1.67 eV (see Table I).

In QSGW, the  $\Delta E_{e_g}$  of both  $\text{La}_2\text{CuO}_4$  and  $\text{HgBa}_2\text{CuO}_4$  is enhanced compared to LDA/GGA. How does this affect the theoretical estimation of  $T_c$ ? First, it should be noted that these parameters cannot be directly adopted as the inputs for the FLEX calculation. This is because, in principle, the QSGW self energy should be partially subtracted before we put it into any of many-body calculations. While there is no well-defined prescription yet for this kind of ‘double-counting’ problem [39], the “best”  $\Delta E_{e_g}$  that should be adopted in the FLEX evaluation of  $T_c$  may be lying somewhere in between the QSGW and LDA/GGA values. This can provide better quantitative agreement with the experiment, especially in  $\text{La}_2\text{CuO}_4$ , for which the LDA/GGA value of  $\Delta E_{e_g}$  is found to be too small to account for  $T_c = 40\text{K}$ .

Oxygen states are also affected. Compared to LDA results, the O-2*p* levels obtained by QSGW are significantly lowered in energy, as indicated in Fig. 2. As summarized in Table I, the center position of in-plane oxygen PDOS is located at  $-4.44$  ( $-3.55$ ) eV in LDA and at  $-5.06$  ( $-4.05$ ) eV in QSGW for  $\text{La}_2\text{CuO}_4$  ( $\text{HgBa}_2\text{CuO}_4$ ). The same feature is found for the apical O-*p<sub>z</sub>* PDOS. As a result, the energy difference,  $\Delta E_p = E_{\text{apical}} - E_{\text{inplane}}$ , is changed from 1.68 (1.00) in LDA to 0.55 ( $-0.86$ ) in QSGW for the case of  $\text{La}_2\text{CuO}_4$  ( $\text{HgBa}_2\text{CuO}_4$ ), see Table I. The correct estimation of  $\Delta E_p$  is also important for understanding  $T_c$  since it is an underlying quantity to determine  $\Delta E_{e_g}$  ( $\approx \Delta E \approx \Delta E_d + \Delta E_p$  [40]) in combination with other parameters.

Some other changes produced by QSGW are also noted. The  $d_{3z^2-r^2}$  components in the bands below  $-1.5$  eV in Fig. 1(a) are reduced in QSGW, and the free-electron-like bands at  $\Gamma$  and  $Z$  points above the Fermi energy are shifted upward. As the position of the  $t_{2g}$  complex is lowered (red color), the  $d_{x^2-y^2}$  band has almost no mixture with other bands below the Fermi energy. Higher-lying La-4*f* bands (not shown) move further upward as has been previously noted in the nickelate systems [41].

## Fermi surface

The shape of the Fermi surface is important for understanding cuprate superconductivity. For example, its nesting is crucial for the spin fluctuation pairing. Also, a notable correlation between the experimentally observed  $T_c$  at the optimal doping ( $T_c^{\text{max}}$ ) and the Fermi surface

warping has been identified by Pavarini *et al.* [24]. Here we discuss the Fermi surface calculated by QSGW in comparison to the LDA result and experiment.

The calculated Fermi surfaces are presented in Fig. 3; LDA ((a, c)) and QSGW ((b, d)). The hole doping is simulated by the rigid band shift method so that the electron occupation in  $e_g$  orbitals is reduced by  $0.15e$  per unit cell. Notable features are found in the QSGW Fermi surface for  $\text{La}_2\text{CuO}_4$ . Contrary to the LDA result of Fig. 3(a), Fig. 3(b) has the pocket centered at  $(\pi, \pi)$  point as in  $\text{HgBa}_2\text{CuO}_4$  Fermi surface (see Fig. 3(c) and (d)). This feature is in good agreement with ARPES data [42] which also reports the pocket centered at  $(\pi, \pi)$  point. Further, the  $d_{3z^2-r^2}$ -orbital character (dark purple) is significantly reduced and the  $d_{x^2-y^2}$  character (bright yellow) is dominant in the QSGW result, which is distinctive from the LDA in which the significant amount of  $d_{3z^2-r^2}$  components are observed near  $(\pi, 0)$  and  $(0, \pi)$ .

In the case of  $\text{HgBa}_2\text{CuO}_4$ , the difference between LDA and QSGW is less pronounced, see Fig. 3(c) and (d). While the QSGW Fermi surface is slightly more rounded, the overall shape is not much different. Since the  $d_{x^2-y^2}$  orbital character is dominant and  $d_{3z^2-r^2}$  band is well separated from Fermi level already in LDA due to the thicker blocking layers enhancing two-dimensional feature, the LDA result is quite similar to QSGW.

### Comparison with RIXS

We now turn to the comparison with the RIXS data. Recently, Sala *et al.* [32] successfully extracted the important model parameters for several different cuprate materials based on RIXS spectra. In this subsection, we examine the material dependent parameters by QSGW and compare them to the experimental values. With Ref. 32 as our main reference, we include two more compounds, namely,  $\text{Sr}_2\text{CuO}_2\text{Cl}_2$  and  $\text{CaCuO}_2$  [43].

Our results are summarized in Table I, Fig. 4, and Fig. 5. The values of  $10Dq$ , defined as the difference between two energy levels of  $d_{x^2-y^2}$  and  $d_{xy}$  (see Fig. 4(a)), are larger in the QSGW calculation by  $\sim 62\text{--}125\%$  than the LDA values. While LDA underestimates  $10Dq$  compared to the experiment, QSGW slightly overestimates, which is related to the tendency that  $\text{Cu-}t_{2g}$  bands are pushed down relative to  $e_g$ , as was also observed in the previous QSGW calculations for other transition-metal oxides [41, 44, 45]. It is important to note that overall the QSGW result is in better agreement with experiment, as clearly

seen in Fig. 4(b).

As noted in the above, according to the two-band theory by Sakakibara *et al.* [26, 27], the important parameter that governs  $T_c$  is  $\Delta E_{e_g}$  (or  $4Ds+5Dt$  in Ref. 32). Fig. 4(b) and Fig. 5 clearly show that the calculated values of  $\Delta E_{e_g}$  by QSGW are in excellent agreement with those from RIXS spectra; the difference is 2–8 %. The LDA values are noticeably smaller than the experiments although the difference gets reduced in the higher  $T_c$  materials,  $\text{CaCuO}_2$  and  $\text{HgBa}_2\text{CuO}_4$  (see Fig. 5). This can be taken as a strong support for the two-band theory in the sense that the LDA value of  $\Delta E_{e_g}$  as an input for FLEX provides qualitative information of material dependence, while the  $\Delta E_{e_g}$  by QSGW already contains the correlation effect beyond LDA, being consistent with RIXS.

Another parameter deduced from RIXS in Ref. 32 is  $3Ds-5Dt$ , the energy level difference between  $d_{xy}$  and  $d_{yz, zx}$ . In this case, the LDA results are not much different from QSGW and experiment (see Fig. 4(b)).

### The effect of epitaxial strain

An interesting aspect found in the  $T_c$  trend of the cuprates is its significant enhancement in the thin film form. Locquet *et al.* reported [46] that  $T_c$  can be controlled by epitaxial strain by about factor of two [47]. The underdoped  $\text{La}_2\text{CuO}_4$  with its bulk  $T_c$  of 25K exhibits a higher and lower  $T_c$  of  $\sim 49$  K and 10 K when it is grown on  $\text{SrLaAlO}_4$  (SLAO) and  $\text{SrTiO}_3$  (STO) substrates, respectively [46]. It is therefore important to check whether the two-band theory is also consistent with this observation.

In order to simulate the tensile and compressive strain produced by STO and SLAO, we first optimized the  $c$  lattice parameter with two different in-plane lattice constants,  $a^{\text{STO}}=3.905$  and  $a^{\text{SLAO}}=3.755$  Å, for  $\text{La}_2\text{CuO}_4$ , which originally has  $a_0=3.782$  Å and  $c_0=13.25$  Å. As expected, the optimized out-of-plane parameters get smaller and larger under the tensile and compressive strain, respectively;  $c_{\text{STO}}^{\text{opt}}=12.96$  and  $c_{\text{SLAO}}^{\text{opt}}=13.36$  Å. As a result, the ratio between the out-of-plane and in-plane Cu–O distance,  $r = d_{\text{apical}}/d_{\text{inplane}}$ , is found to be 1.32, 1.28, and 1.24, for  $a^{\text{SLAO}}$ ,  $a_0$  and  $a^{\text{STO}}$ , respectively.

The calculated values of  $\Delta E_{e_g}$  are plotted in Fig. 6. Both LDA and QSGW predict that  $\Delta E_{e_g}$  gets enhanced and reduced under compressive and tensile strain, respectively, which is consistent with the experimental observation [46]. The reduction of  $\Delta E_{e_g}$  at  $a=a_{\text{STO}}$  is

about 0.16 eV in both LDA and QSGW, and the enhancement at  $a=a_{\text{SLAO}}$  is 0.29 (LDA) and 0.47 eV (QSGW).

## Summary and Conclusion

Using the QSGW method, we re-examined the electronic structure of copper oxide high temperature superconducting materials. Several important features were found to have been captured by the  $GW$  procedure, such as effective mass enhancement. The shape and orbital character of the Fermi surface were also notably changed, especially for the case of  $\text{La}_2\text{CuO}_4$ , and they are in good agreement with the ARPES data [42]. Important model parameters including the key quantity for the two-band theory of  $T_c$ ,  $\Delta E_{eg}$ , were examined, and the QSGW results were in excellent agreement with RIXS data.

The present study shows that the first-principles band calculation can quantitatively reproduce the experimental observation by taking into account the correlation effects beyond LDA. We emphasize that it is not inconsistent with the previous study by Sakakibara *et al.* which takes the LDA result as an input for the many-body calculation of superconductivity. While the QSGW result cannot be used as a direct input for the FLEX-type calculation because of the partial double-counting of the many-body correlation, the “best” non-interacting Hamiltonian, that can serve as an input, may lie somewhere in between the LDA and QSGW. Obtaining a well-defined non-interacting Hamiltonian is, therefore, an important future direction for the first-principles-based description of high-temperature superconductivity, and it may quantitatively resolve the problem of low  $T_c$  in  $\text{La}_2\text{CuO}_4$  produced by the LDA input [33].

## Methods

### Quasiparticle self-consistent $GW$

The QSGW [44, 45, 48] calculates  $H_0$  (non-interacting Hamiltonian describing quasiparticles or band structures) and  $W$  (dynamically-screened Coulomb interactions between the quasiparticles within the random phase approximation) in a self-consistent manner. While the ‘one-shot’  $GW$  is a perturbative calculation starting from a given  $H_0$  (usually from



LDA/GGA), QSGW is a self-consistent perturbation method that can determine the one-body Hamiltonian within itself. The  $GW$  approximation gives the one-particle effective Hamiltonian whose energy dependence comes from the self-energy term  $\Sigma(\omega)$  (here we omit index of space and spin for simplicity), and in QSGW, the static one-particle potential  $V^{\text{xc}}$  is generated as

$$V^{\text{xc}} = \frac{1}{2} \sum_{ij} |\psi_i\rangle \{ \text{Re}[\Sigma(\varepsilon_i)]_{ij} + \text{Re}[\Sigma(\varepsilon_j)]_{ij} \} \langle \psi_j|, \quad (1)$$

where  $\varepsilon_i$  and  $|\psi_i\rangle$  refer to the eigenvalues and eigenfunctions of  $H_0$ , respectively, and  $\text{Re}[\Sigma(\varepsilon)]$  is the Hermitian part of the self-energy [44, 45, 48]. With this  $V^{\text{xc}}$ , one can define a new static one-body Hamiltonian  $H_0$ , and continue to apply  $GW$  approximation until converged. In principle, the final result of QSGW does not depend on the initial conditions. Previous QSGW studies, ranging from semiconductors [44, 45] to the various  $3d$  transition metal oxides [44, 45, 49] and  $4f$ -electron systems [50], have demonstrated its capability in the description of weakly and strongly correlated electron materials.

### Computation details

We used our new implementation of QSGW [51] by adopting the ‘augmented plane wave (APW) + muffin-tin orbital (MTO)’, designated by ‘PMT’ [52, 53], for the one-body solver. The accuracy of this full potential PMT method is proven to be satisfactory in the supercell calculations of homo-nuclear dimers from  $\text{H}_2$  through  $\text{Kr}_2$  with the significantly low APW energy cutoff of  $\sim 4$  Ry, by including localized MTOs [53]. A key feature of this scheme for QSGW is that the expansion of  $V^{\text{xc}}$  can be made with MTOs, not APWs, which enables us to make the real space representation of  $V^{\text{xc}}$  at any  $\mathbf{k}$  point.

We performed the calculations with the experimental crystal structures [54–57], and used  $10 \times 10 \times 10$ ,  $12 \times 12 \times 12$ ,  $12 \times 12 \times 8$ , and  $14 \times 14 \times 14$   $\mathbf{k}$  points for LDA calculations of  $\text{Sr}_2\text{CuO}_2\text{Cl}_2$ ,  $\text{La}_2\text{CuO}_4$ ,  $\text{HgBa}_2\text{CuO}_4$ , and  $\text{CaCuO}_2$ , respectively. As for QSGW calculations, in order to reduce the computation cost, the number of  $\mathbf{k}$  points were reduced to be  $5 \times 5 \times 5$ ,  $7 \times 7 \times 7$ ,  $8 \times 8 \times 4$ , and  $8 \times 8 \times 8$  for the first Brillouin zone of  $\text{Sr}_2\text{CuO}_2\text{Cl}_2$ ,  $\text{La}_2\text{CuO}_4$ ,  $\text{HgBa}_2\text{CuO}_4$ , and  $\text{CaCuO}_2$ , respectively. The MTO radii used in our calculations were as follows: (i) 1.58, 1.04, 0.89, and 1.38 Å for Sr, Cu, O, and Cl in  $\text{Sr}_2\text{CuO}_2\text{Cl}_2$ , (ii) 1.43, 0.97, and 0.86 Å for La, Cu, and O in  $\text{La}_2\text{CuO}_4$ , (iii) 1.10, 1.59, 1.05, and 0.83 Å for Hg, Ba, Cu,

and O in  $\text{HgBa}_2\text{CuO}_4$ , and (iv) 1.54, 1.01, and 0.86 for Ca, Cu, and O in  $\text{CaCuO}_2$ .

Many of the key parameters in this study are defined in terms of the energy levels of each orbital, such as  $E_{x^2-y^2}$  and  $E_{3z^2-r^2}$ . To quantify them we simply take the center of mass position of PDOS:

$$E_\alpha = \frac{\int_{E_{\min}}^{E_{\max}} E g_\alpha(E) dE}{\int_{E_{\min}}^{E_{\max}} g_\alpha(E) dE}, \quad (2)$$

where  $g_\alpha(E)$  is PDOS for a given orbital  $\alpha$ . An ambiguity is inevitably introduced in determining  $E_{\min, \max}$ , and we set the range to cover the whole antibonding band complex for Cu- $e_g$  states. ( $E_{\min}^{e_g}$ ,  $E_{\max}^{e_g}$ ) for  $\text{La}_2\text{CuO}_4$  is (-1.95 eV, 2.05 eV) in LDA and (-2.20, 1.55) in QSGW. For  $\text{HgBa}_2\text{CuO}_4$ , the band dispersion changes and the values of  $E_{\min}^{e_g}$  and  $E_{\max}^{e_g}$  are redefined accordingly: ( $E_{\min}^{e_g}$ ,  $E_{\max}^{e_g}$ )=(-2.40, 2.50) in LDA and (-2.55, 1.65) in QSGW. Importantly, none of the reasonably defined energy ranges change our conclusion [58], and the values are well compared with those reported in the previous study using a maximally localized Wannier function [26, 27].

- 
- [1] Bednorz, J. G. & Müller, K. A. Possible high  $T_c$  superconductivity in the Ba-La-Cu-O system. *Z. Phys. B: Condens. Matter* **64**, 189–193 (1986).
  - [2] Norman, M. R., Pines, D., & Kallin, C. The pseudogap: friend or foe of high  $T_c$ ? *Adv. Phys.* **54**, 715–733 (2005).
  - [3] Lee, P. A., Nagaosa, N. & Wen, X. -G. Doping a Mott insulator: Physics of high-temperature superconductivity. *Rev. Mod. Phys.* **78**, 17–85 (2006).
  - [4] Lee, P. A. From high temperature superconductivity to quantum spin liquid: progress in strong correlation physics. *Rep. Prog. Phys.* **71**, 012501 (2008).
  - [5] Ogata, M. & Fukuyama, H. The  $t$ - $J$  model for the oxide high- $T_c$  superconductors. *Rep. Prog. Phys.* **71**, 036501 (2008).
  - [6] Hübner, S., Hossain, M. A. , Damascelli, A. & Sawatzky, G. A. Two gaps make a high-temperature superconductor? *Rep. Prog. Phys.* **71**, 062501 (2008).
  - [7] Barzykin, V. & Pines, D. Universal behaviour and the two-component character of magnetically underdoped cuprate superconductors. *Adv. Phys.* **58**, 1–65 (2009).

- [8] Vojta, M. Lattice symmetry breaking in cuprate superconductors: stripes, nematics, and superconductivity. *Adv. Phys.* **58**, 699–820 (2009).
- [9] Alloul, H., Bobroff, J., Gabay, M. & Hirschfeld, P. J. Defects in correlated metals and superconductors. *Rev. Mod. Phys.* **81**, 45–108 (2009).
- [10] Armitage, N. P., Fournier, P. & Greene, R. L. Progress and perspectives on electron-doped cuprates. *Rev. Mod. Phys.* **82**, 2421–2487 (2010).
- [11] Scalapino, D. J. A common thread: The pairing interaction for unconventional superconductors. *Rev. Mod. Phys.* **84**, 1383–1417 (2012).
- [12] Fradkin, E., Kivelson, S. A. & Tranquada, J. M., Theory of intertwined orders in high temperature superconductors. *arxiv:1407.4480* (2014).
- [13] Weber, C., Haule, K. & Kotliar, G. Apical oxygens and correlation strength in electron- and hole-doped copper oxides. *Phys. Rev. B* **82**, 125107 (2010).
- [14] Weber, C., Yee, C., Haule, K. & Kotliar, G. Scaling of the transition temperature of hole-doped cuprate superconductors with the charge-transfer energy. *Eur. Phys. Lett.* **100**, 37001 (2012).
- [15] Takimoto, T., Hotta, T. & Ueda, K. Strong-coupling theory of superconductivity in a degenerate Hubbard model. *Phys. Rev. B* **69**, 104504 (2004).
- [16] Wang, X., Dang, H. T. & Millis, A. J.  $d_{3z^2-r^2}$  orbital in high- $T_c$  cuprates: Excitonic spectrum, metal-insulator phase diagram, optical conductivity, and orbital character of doped holes. *Phys. Rev. B* **84**, 014530 (2011).
- [17] Hozoi, L., Siurakshina, L., Fulde, P. & van den Brink, J. *Ab Initio* determination of Cu 3d orbital energies in layered copper oxides. *Sci. Rep.* **1**, 65 (2011).
- [18] Uebelacker, S. & Honerkamp, C. Multiband effects on superconducting instabilities driven by electron-electron interactions. *Phys. Rev. B* **85**, 155122 (2012).
- [19] Mori, M., Khaliullin, G., Tohyama, T. & Maekawa, S. Origin of the spatial variation of the pairing gap in Bi-based high temperature cuprate superconductors. *Phys. Rev. Lett.* **101**, 247003 (2008).
- [20] Ohta, Y., Tohyama, T. & Maekawa, S. Apex oxygen and critical temperature in copper oxide superconductors: Universal correlation with the stability of local singlets. *Phys. Rev. B* **43**, 2968–2982 (1991).
- [21] Maekawa, S., Inoue, J. & Tohyama, T. *The Physics and Chemistry of Oxide Superconductors*

- [Iye, Y. & Yasuoka, H. (ed.)] [105–115] (Springer-Verlag, Berlin, 1992).
- [22] Feiner, L. F., Jefferson, J. H. & Raimondi, R. Intracublattice hopping in the extended  $t$ - $J$  model and  $T_c^{\max}$  in the cuprates. *Phys. Rev. Lett.* **76**, 4939–4942 (1996).
- [23] Hozoi, L. & Laad, M. S. Quasiparticle bands in cuprates by quantum-chemical methods: towards an *Ab initio* description of strong electron correlations *Phys. Rev. Lett.* **99**, 256404 (2007).
- [24] Pavarini, E., Dasgupta, I., Saha-Dasgupta, T., Jepsen, O. & Anderson, O. K. Band-Structure Trend in Hole-Doped Cuprates and Correlation with  $T_{c \max}$ . *Phys. Rev. Lett.* **87**, 047003 (2001).
- [25] Andersen, O. K., Liechtenstein, A. I., Jepsen, O. & Paulsen, F. LDA energy bands, low-energy Hamiltonians  $t'$ ,  $t''$ ,  $t_{\perp}(\mathbf{k})$ , and  $J_{\perp}$ . *J. Phys. Chem. Solids* **56**, 1573–1591 (1995).
- [26] Sakakibara, H., Usui, H., Kuroki, K., Arita, R. & Aoki, H. Two-orbital model explains the higher transition temperature of the single-layer Hg-cuprate superconductor compared to that of the La-cuprate superconductor. *Phys. Rev. Lett.* **105**, 057003 (2010).
- [27] Sakakibara, H., Usui, H., Kuroki, K., Arita, R. & Aoki, H. Origin of the material dependence of  $T_c$  in the single-layered cuprates. *Phys. Rev. B* **85**, 064501 (2012).
- [28] Sakakibara, H. *et al.* Multiorbital analysis of the effects of uniaxial and hydrostatic pressure on  $T_c$  in the single-layered cuprate superconductors. *Phys. Rev. B* **86**, 134520 (2012).
- [29] Sakakibara, H. *et al.* Orbital mixture effect on the Fermi-surface- $T_c$  correlation in the cuprate superconductors: Bilayer vs. single layer. *Phys. Rev. B* **89**, 224505 (2014).
- [30] Bickers, N. E., Scalapino, D. J. & White, S. R. Conserving approximations for strongly correlated electron systems: Bethe-Salpeter equation and dynamics for the two-dimensional Hubbard model. *Phys. Rev. Lett.* **62**, 961–964 (1989).
- [31] Dahm, T. & Tewordt, L. Quasiparticle and spin excitation spectra in the normal and d-wave superconducting of the two-dimensional Hubbard model. *Phys. Rev. Lett.* **74**, 793–796 (1995).
- [32] Moretti Sala, M. *et al.* Energy and symmetry of dd excitations in undoped layered cuprates measured by Cu  $L_3$  resonant inelastic x-ray scattering. *New Jour. Phys.* **13**, 043026 (2011).
- [33] Miyahara, H., Arita, R. & Ikeda, H. Development of a two-particle self-consistent method for multiorbital systems and its application to unconventional superconductors. *Phys. Rev. B* **87**, 045113 (2013). In this paper, it is shown that the LDA+FLEX approach cannot account for  $T_c = 40\text{K}$  for  $\text{La}_2\text{CuO}_4$ , and this problem can be resolved by adopting the two particle

self-consistent method instead of FLEX.

- [34] Biermann, S., Aryasetiawan, F. & Georges, A., First-principles approach to the electronic structure of strongly correlated systems: combining the  $GW$  approximation and dynamical mean-field theory. *Phys. Rev. Lett.* **90**, 086402 (2003).
- [35] Sun, P. & Kotliar, G. Many-body approximation scheme beyond  $GW$ . *Phys. Rev. Lett.* **92**, 196402 (2004).
- [36] Ayrál, T., Werner, P. & Biermann, S. Spectral properties of correlated materials: Local vertex and nonlocal two-particle correlations from combined  $GW$  and dynamical mean field theory. *Phys. Rev. Lett.* **109**, 226401 (2012).
- [37] Ayrál, T., Biermann, S. & Werner, P. Screening and nonlocal correlations in the extended Hubbard model from self-consistent combined  $GW$  and dynamical mean field theory. *Phys. Rev. B* **87**, 125149 (2013).
- [38] Das, T., Markiewicz, R. S. & Bansil, A. Intermediate coupling model of the cuprates. *Adv. Phys.* **63**, 151 (2014).
- [39] See, for example, Wang, X. *et al.* Covalency, double-counting, and the metal-insulator phase diagram in transition metal oxides. *Phys. Rev. B* **86**, 195136 (2012).
- [40] Our  $\Delta E_{e_g}$  is different from  $\Delta E_d$  and  $\Delta E$  in Ref. 26–29 where  $\Delta E \approx \Delta E_d + \Delta E_p$ ,  $\Delta E_d = E_{x^2-y^2} - E_{3z^2-r^2}$ ,  $\Delta E_p = E_{\text{apical}}^{\text{O}} - E_{\text{inplane}}^{\text{O}}$ , and all of the parameters are calculated from the maximally localized Wannier orbital analysis. The  $\Delta E$  contains the contribution from oxygen hybridization. We note, however, that our  $\Delta E_{e_g}$  becomes effectively quite similar with  $\Delta E$  in Ref. 26–29 since we set our  $E_{\text{min,max}}$  to cover only the anti-bonding band complex. Actually one can make it almost equal, *i.e.*,  $\Delta E_{e_g} \approx \Delta E$ , by fine-tuning the  $E_{\text{min,max}}$  range.
- [41] Han, M. J., Kino, H. & Kotani, T. Quasiparticle self-consistent  $GW$  study of  $\text{LaNiO}_3$  and  $\text{LaNiO}_3/\text{LaAlO}_3$  superlattice. *Phys. Rev. B* **90**, 035127 (2014).
- [42] Ino, A. *et al.* Doping-dependent evolution of the electronic structure of  $\text{La}_{2-x}\text{Sr}_x\text{CuO}_4$  in the superconducting and metallic phases. *Phys. Rev. B* **65**, 094504 (2002).
- [43] Although  $\text{Sr}_2\text{CuO}_2\text{Cl}_2$  is also one of the single-layer cuprates, it has  $\text{Cl-Cu-Cl}$  bonding (instead of  $\text{O-Cu-O}$ ) along  $c$ -axis and therefore the naive comparison of parameters such as  $\Delta E_{e_g}$  and  $\Delta E_p$  in the line of  $T_c$  discussion may be misleading. This material is excluded in Ref. 26–29 because of the same reason.
- [44] van Schilfhaarde, M., Kotani, T. & Falëev, S. Quasiparticle self-consistent  $GW$  theory. *Phys.*

- Rev. Lett.* **96**, 226402 (2006).
- [45] Kotani, T., van Schilfgaarde, M. & Faleev, S. V. Quasiparticle self-consistent *GW* method: A basis for the independent-particle approximation. *Phys. Rev. B* **76**, 165106 (2007).
- [46] Locquet, J.-P. *et al.* Doubling the critical temperature of  $\text{La}_{1.9}\text{Sr}_{0.1}\text{CuO}_4$  using epitaxial strain. *Nature* **394**, 453–456 (1998).
- [47] See also, Bozovic, I., Logvenov, G., Belca, I., Narimbetov, B. & Sveklo, I., Epitaxial strain and superconductivity in  $\text{La}_{2-x}\text{Sr}_x\text{CuO}_4$  thin films. *Phys. Rev. Lett.* **89**, 107001 (2002).
- [48] Faleev, S. V., van Schilfgaarde, M. & Kotani, T. All-electron self-consistent *GW* approximation: Application to Si, MnO, and NiO. *Phys. Rev. Lett.* **93**, 126406 (2004).
- [49] Kotani, T. & van Schilfgaarde, M. Spin wave dispersion based on the quasiparticle self-consistent *GW* method: NiO, MnO and  $\alpha$ -MnAs. *J. Phys.: Condens. Matter* **20**, 295214 (2008).
- [50] Chantis, A. N., van Schilfgaarde, M. & Kotani, T. Quasiparticle self-consistent *GW* method applied to localized 4f electron systems. *Phys. Rev. B* **76**, 165126 (2007).
- [51] Kotani, T. Quasiparticle self-consistent *GW* method based on the augmented plane-wave and muffin-tin orbital method. *J. Phys. Soc. Jpn.* **83**, 094711 (2014).
- [52] Kotani, T. & van Schilfgaarde, M. Fusion of the LAPW and LMTO methods: The augmented plane wave plus muffin-tin orbital method. *Phys. Rev. B* **81**, 125117 (2010).
- [53] Kotani, T. & Kino, H. Linearized augmented plane-wave and muffin-tin orbital method with the PBE exchange-correlation: Applied to molecules from  $\text{H}_2$  through  $\text{Kr}_2$ . *J. Phys. Soc. Jpn.* **82**, 124714 (2013).
- [54] Miller, L. L., Wang, X. L., Wang, S. X., Stassis, C. & Johnston, D. C. Synthesis, structure, and properties of  $\text{Sr}_2\text{CuO}_2\text{Cl}_2$ . *Phys. Rev. B* **41**, 1921–1925 (1990).
- [55] Jorgensen, J. D. *et al.* Lattice instability and high- $T_c$ , superconductivity in  $\text{La}_{2-x}\text{Ba}_x\text{CuO}_4$ . *Phys. Rev. Lett.* **58**, 1024–1027 (1987).
- [56] Wagner, J. L. *et al.* Structure and superconductivity of  $\text{HgBa}_2\text{CuO}_{4+\delta}$ . *Physica C* **210**, 447–454 (1993).
- [57] Qin, X. M. *et al.* The high-pressure synthesis and in situ property of the infinite-layer  $\text{CaCuO}_2$ . *Physica C* **426-431**, 510 (2005).
- [58] If we choose two different ranges for two  $e_g$  orbitals to include only the main peak of each orbital PDOS, we can actually produce the better agreement with the numbers in the previous study

by Sakakibara *et al.* where the levels are defined using maximally localized Wannier function method. Even if the ranges are set to cover the whole window of Cu- $e_g$  bands including bonding parts, the trend reported in this work does not change. The same is true for O- $2p$  and Cu- $t_{2g}$  levels.

### **Acknowledgments**

We thank Ryotaro Arita for helpful comment and Prof. Hiroshi Katayama-Yoshida for hosting the helpful discussion. S.W.J. and M.J.H. were supported by Basic Science Research Program through the National Research Foundation of Korea(NRF) funded by the Ministry of Education(2014R1A1A2057202). The computing resource is supported by National Institute of Supercomputing and Networking / Korea Institute of Science and Technology Information with supercomputing resources including technical support (KSC-2014-C3-050) and by Computing System for Research in Kyushu University.

### **Author contributions**

S.W.J., T.K., and H.K. performed the calculations. All authors contributed in analyzing the results and writing the paper.

### **Additional information**

The authors declare that they have no competing financial interests.

## Tables

TABLE I: The calculated parameters by LDA and QSGW. The  $p_{x,y}$  is from the in-plane oxygen, and  $p_z$  from the out-of-plane. The definitions of parameters can be found in Fig. 4. The experimental values are taken from Ref. 32.

	$E_{d_{x^2-y^2}} - E_{\text{Fermi}}$ (eV)		$E_{d_{z^2}} - E_{\text{Fermi}}$ (eV)		$E_{O_{p_{x,y}}} - E_{\text{Fermi}}$ (eV)		$E_{O_{p_z}} - E_{\text{Fermi}}$ (eV)		
	LDA	QSGW	LDA	QSGW	LDA	QSGW	LDA	QSGW	
$\text{Sr}_2\text{CuO}_2\text{Cl}_2$	-0.29	0.01	-1.23	-2.05	-4.67	-4.92	-3.61	-5.44	
$\text{La}_2\text{CuO}_4$	-0.14	-0.03	-0.98	-1.68	-4.44	-5.06	-2.76	-4.06	
$\text{HgBa}_2\text{CuO}_4$	-0.20	-0.05	-1.87	-2.30	-3.55	-4.05	-3.00	-4.91	
$\text{CaCuO}_2$	-0.30	-0.17	-2.34	-2.63	-3.67	-4.05	None	None	
	$\Delta E_{e_g}$ (4Ds + 5Dt) (eV)			3Ds - 5Dt (eV)			10Dq (eV)		
	LDA	QSGW	Exp (Ref. 32)	LDA	QSGW	Exp (Ref. 32)	LDA	QSGW	Exp (Ref. 32)
$\text{Sr}_2\text{CuO}_2\text{Cl}_2$	0.94	2.05	1.97	0.22	0.21	0.33	0.81	1.82	1.50
$\text{La}_2\text{CuO}_4$	0.84	1.66	1.70	0.17	0.11	0.32	1.47	2.13	1.80
$\text{HgBa}_2\text{CuO}_4$	1.67	2.25	None	0.42	0.42	None	0.90	1.57	None
$\text{CaCuO}_2$	2.04	2.46	2.65	0.05	0.28	0.31	0.92	1.69	1.64



## Figure Legends

FIG. 1: The band dispersion and PDOS of  $\text{La}_2\text{CuO}_4$  (a, b) and  $\text{HgBa}_2\text{CuO}_4$  (c, d) calculated by (a, c) LDA and (b, d) QSGW. The green and blue colors refer to the  $d_{x^2-y^2}$  and  $d_{3z^2-r^2}$  characters while the size of the colored dots represents their weight. The same color scheme was used for PDOS. Other bands than the two  $e_g$  states are represented by red color. The center of mass position of PDOS is marked by an arrow. Fermi energy is set to be 0.

FIG. 2: The calculated oxygen PDOS of  $\text{La}_2\text{CuO}_4$  by LDA and QSGW. (a) In-plane oxygen  $p_{x,y}^\sigma$  and (b) out-of-plane oxygen  $p_z^\sigma$  orbitals are plotted. The center of mass position of each PDOS is marked by an arrow. Fermi energy is set to be 0.

FIG. 3: The orbital-resolved Fermi surfaces ( $k_z=0$  plane) at the reduced  $e_g$  band filling by 0.15 (hole doping): (a)  $\text{La}_2\text{CuO}_4$  (LDA), (b)  $\text{La}_2\text{CuO}_4$  (QSGW), (c)  $\text{HgBa}_2\text{CuO}_4$  (LDA), and (d)  $\text{HgBa}_2\text{CuO}_4$  (QSGW). The color represents the amount of  $d_{x^2-y^2}$  and  $d_{3z^2-r^2}$  character.

FIG. 4: (a) The three model parameters for the comparison to Ref. 32. Note that  $\Delta E_{e_g}$  is denoted by  $4Ds + 5Dt$  in Ref. 32. (b) The difference of the calculated model parameters ( $E_{\text{cal}}$ ) from the experiments ( $E_{\text{exp}}$ ).

FIG. 5: The values of  $\Delta E_{e_g}$  (or  $4Ds + 5Dt$  in the notation of Ref.32) estimated by LDA (blue squares), QSGW (red triangles), and RIXS data (green circles).

FIG. 6: The calculated  $\Delta E_{e_g}$  as a function of epitaxial strain. The  $a_0=3.782 \text{ \AA}$  is the experimental value for bulk  $\text{La}_2\text{CuO}_4$ . The compressive and tensile strain are simulated with  $a = 3.755$  and  $3.905 \text{ \AA}$  considering the substrate of  $\text{SrLaAlO}_4$  and  $\text{SrTiO}_3$ , respectively [46].

# Figures

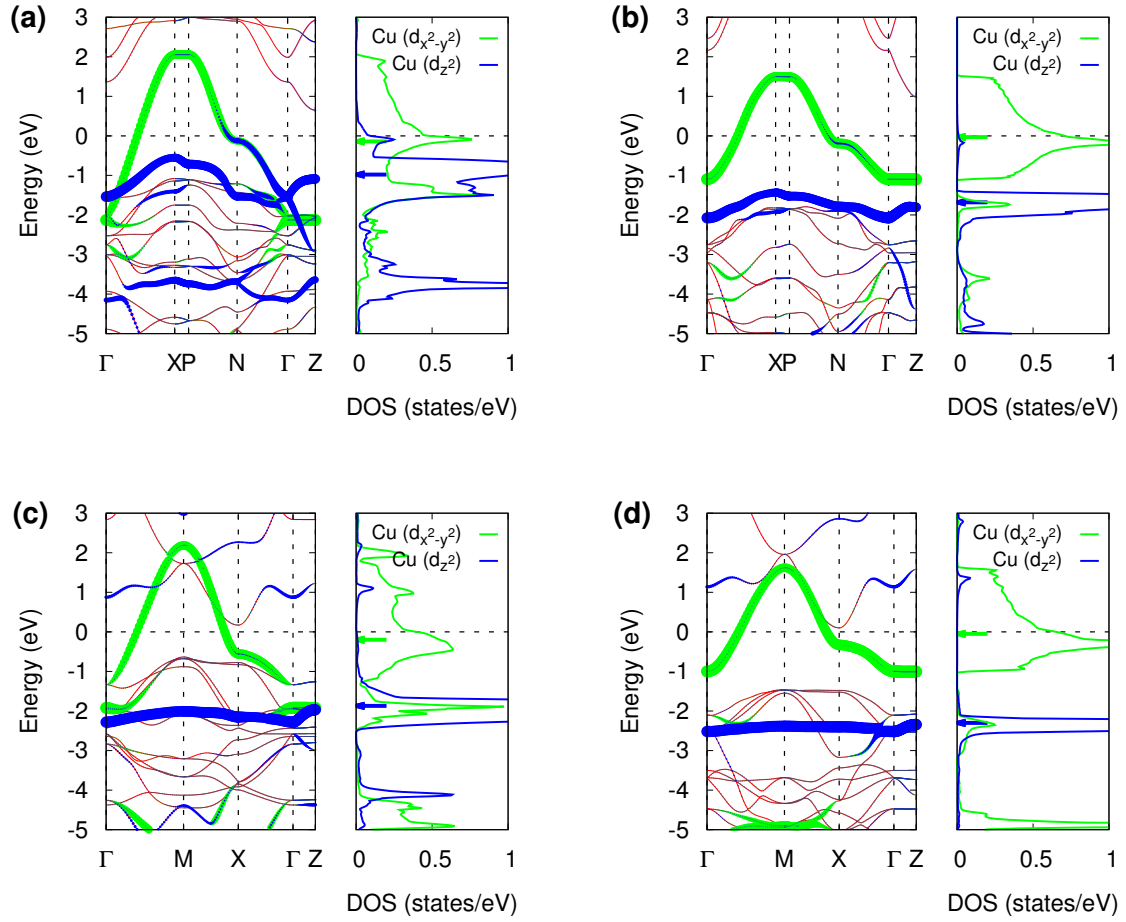


FIG. 1:

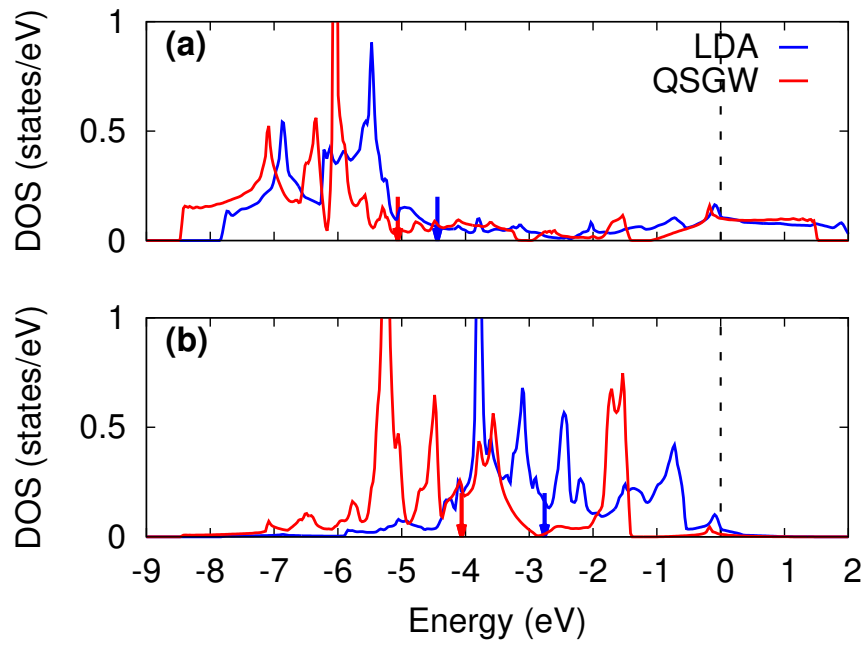


FIG. 2:

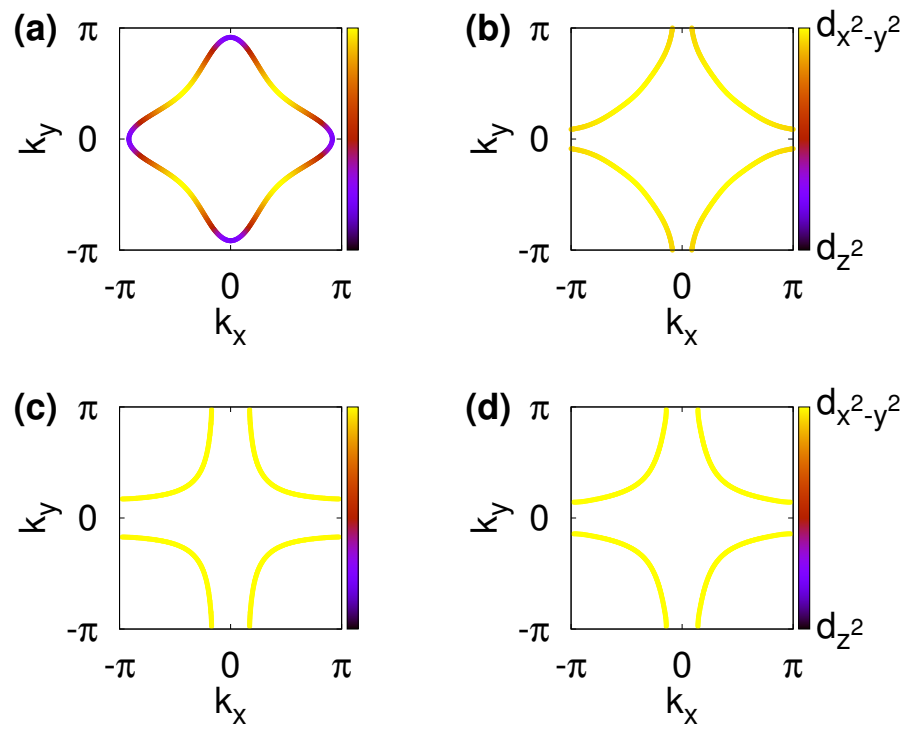


FIG. 3:

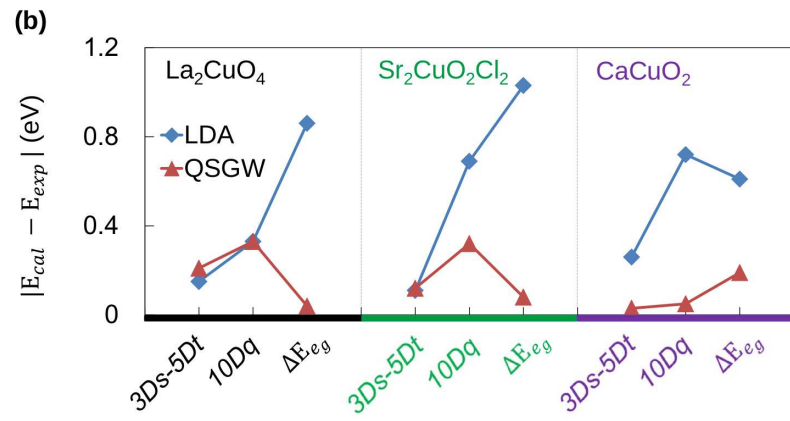
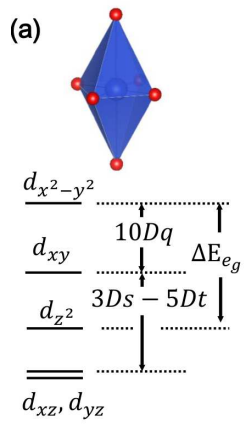


FIG. 4:

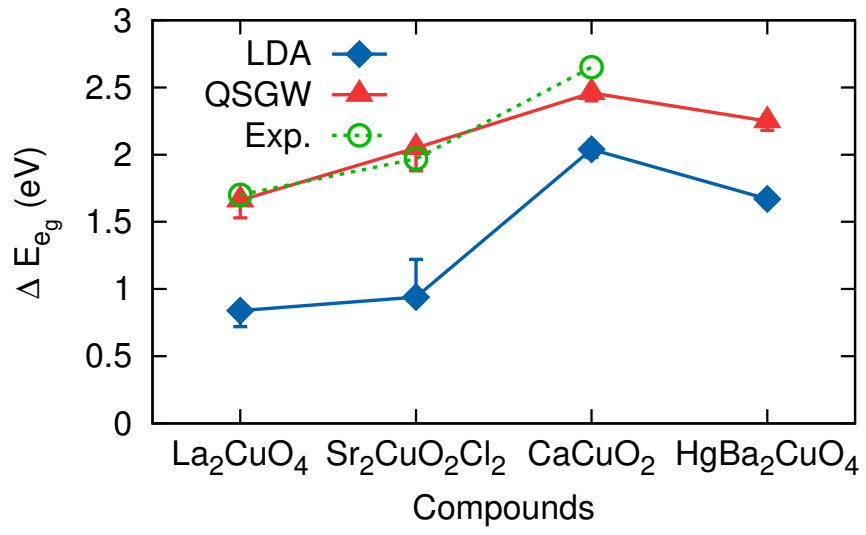


FIG. 5:

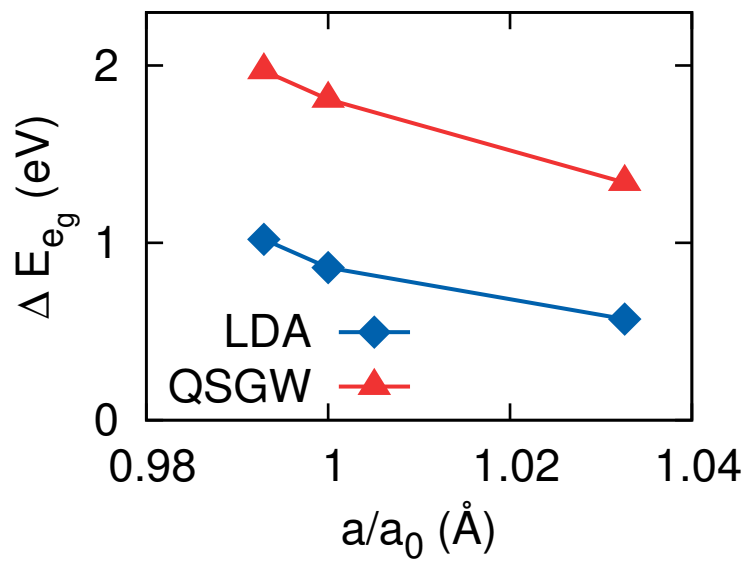


FIG. 6: